**Revista de Metalurgia**
January-March 2021, 57 (1), e189
ISSN-L: 0034-8570
https://doi.org/10.3989/revmetalm.189

# Thermal analysis and wear behavior of shell mold cast and graphite mold cast Mg-4Zn-(x)Zr alloys

Levent Cenk Kumruoglu

Iskenderun Technical University, Faculty of Natural Science and Engineering, 31200 Hatay, Turkey

(*Corresponding author: cenk.kumruoglu@iste.edu.tr)

Submitted: 26 May 2020; Accepted: 14 January 2021; Available On-line: 8 April 2020

**ABSTRACT:** The grain refining effect of Zirconium (Zr) is known, nevertheless the effect of Zr amount and its effect on solidification and wear behavior of modified Mg-Zn alloys has not been adequately studied. Mg-4Zn-(x)Zr alloys alloyed with the addition of 0.5 wt.% to 4 wt.% Zr element are melted and poured into two different casting molds and thermal analyzes were performed. Casting microstructure, solidification behavior, phase transformations, grain size, thermal analysis curves and wear properties were examined. The microstructure was modified by the addition of Zr and the grain size was reduced for both graphite and ceramic mold materials. Maximum tensile strength was obtained by adding 1% Zr (170 MPa) and 4Zr (105-110 HRB) using graphite mold, respectively. The maximum room temperature tensile strength was achieved on the Mg-4Zn-1Zr alloy the elongation was 4.9 percent and the tensile strength was 138 MPa. The max hot tensile value was achieved on the 2 wt% Zr added alloys. The wear rate of Mg–4Zn alloy decreased with increasing Zr element up to 2 wt% Zr. Addition of more than 2% by weight of Zr caused an increase in microporosity in the microstructure. Due to the microporosity caused by the Zr addition, the wear rate was slightly reduced.

**KEYWORDS:** Ceramic mold casting; Die casting; Gravity casting; Mg alloys; Mg-4Zn-(x)Zr alloy; Solidification; Tensile test; Wear properties

**Citation/Citar como:** Kumruoglu, L.C. (2021). "Thermal analysis and wear behavior of shell mold cast and graphite mold cast Mg-4Zn-(x)Zr alloys". *Rev. Metal.* 57(1): e189. https://doi.org/10.3989/revmetalm.189

**RESUMEN:** *Análisis térmico y comportamiento de desgaste de aleaciones Mg-4Zn-(x)Zr fundidos en molde de cáscara y molde de grafito*. El efecto de refinamiento del grano del circonio (Zr) es conocido, sin embargo, la influencia en la cantidad de Zr y su efecto sobre la solidificación y el comportamiento de desgaste de las aleaciones de Mg-Zn modificadas no se han estudiado adecuadamente. Las aleaciones de Mg-4Zn-(x)Zr son aleadas con la adición de 0,5% a 4% en peso de elemento Zr se funden y se vierten en dos moldes de colada diferentes y se realizan análisis térmicos. Se examinaron la microestructura de los productos de colada, el comportamiento de solidificación, las transformaciones de fase, el tamaño de grano, las curvas de análisis térmico y las propiedades de desgaste. La microestructura se modificó mediante la adición de Zr y el tamaño de grano se redujo tanto para los materiales de moldeo de grafito como de cerámica. La máxima resistencia a la tracción se obtuvo añadiendo 1% de Zr (170 MPa) y 4% Zr (105-110 HRB) utilizando un molde de grafito, respectivamente. La máxima resistencia a la tracción a temperatura ambiente se alcanzó en el Mg-4Zn-1Zr, el alargamiento fue del 4,9% y la resis-

tencia a la tracción fue de 138 MPa. El valor máximo de tracción en caliente se obtuvo en las aleaciones con 2% de Zr añadido. La tasa de desgaste de la aleación Mg-4Zn disminuyó al aumentar el elemento Zr hasta un 2% en peso. La adición de más del 2% en peso de Zr provocó un aumento de la microporosidad en la microestructura. Debido a la microporosidad causada por la adición de Zr, la tasa de desgaste se redujo ligeramente.

**PALABRAS CLAVE:** Aleaciones de magnesio; Aleación de Mg-4Zn-Zr; Ensayo de tracción; Fundición por gravedad; Fundición a presión; Fundición de moldes de cerámica; Propiedades de desgaste; Solidificación

**ORCID ID:** Levent Cenk Kumruoglu (https://orcid.org/0000-0001-6420-3761)



## 1. INTRODUCTION

Magnesium and its alloys are of great potential in the electronic, computer, biomedical, structural, and automotive industries because of their superior specific strength property (Kurnaz *et al.*, 2011; Cai *et al.*, 2012; Srinivasan *et al.*, 2014; Jamesh *et al.*, 2015; Yarkadaş *et al.*, 2018; Song *et al.*, 2020). As is known, Magnesium alloys with a density of 1.7 $g \cdot cm^{-3}$ are lighter than other low-density metals such as Titanium and Aluminum. The use of magnesium alloy as a structure material for vehicles is could reduce energy consumption (Barber, 2004; Chalisgaonkar, 2020). Mg alloys are frequently manufactured by different casting techniques. The most common techniques are high-pressure die casting using metal mold (Watarai, 2006; Dadić *et al.*, 2019; Özarslan *et al.*, 2019) and gravity casting using sand mold (Bazhenov *et al.*, 2020; Ren *et al.*, 2011). Because of zirconium presence (applied in order to grain refinement), Mg alloys can be sand casted (Dobrzanski *et al.*, 2009; Zhou *et al.*, 2020). Shell Mold Casting (SMC) is a similar metal casting process by pouring molten metal into an expendable sand-based mold, casting it into a thin-walled shell created by applying a sand-resin mixture around a pattern. The SMC allows higher production rates, while disposable SMC molds allow complex geometries to be cast. Compared to sand casting, The SMC has better dimensional accuracy, higher productivity and lower labor requirements. It is generally used for the production of precision machine elements that require high precision (NovaCast, 2020). The SMC is used for ferrous and non-ferrous metals. The SMC process has some disadvantages, including: Low material strength compared to other casting processes. Shrinkage can be a problem. Porosity can be an issue. Although the surface quality is better than sand casting, it may generally require secondary finish (NovaCast, 2020). Graphite Mold Casting is a niche procedure for casting zinc-aluminum alloy parts. The graphite mold system offers a lower cost tooling alternative than pressure casting. Graphite mold can be processed easily and quickly with CNC machines. These properties make the castings produced with the graphite mold technique more advantageous than sand casting. It allows to produce both low-cost and high-quality parts compared to other casting techniques (Peterson Enterprises, 2020). Graphite is extremely stable: it does not react with molten metal and cast products can be cast with high surface precision. Graphite molds can be stored indefinitely without deformation, rust, oxidation or deterioration. At the same time, graphite has high thermal conductivity. In this way, it provides rapid solidification of the liquid metal after casting and increases nucleation. In this way, the strength is increased by obtaining a fine-grained micro structure. This study was carried out to gain knowledge about the use of magnesium alloys as an alternative molding material in casting. These mold materials are shell molds and graphite molds that can be used industrially and are economical. Mg-4Zn alloy castings produced by using both mold materials were evaluated on the basis of mechanical and wear properties. In addition, Zirconium was added to the Mg-4Zn alloy and its effects on engineering properties were investigated.

Zinc is the second element that is used to alloy that affects the strength, castability, eutectic phase of grain boundary, corrosion resistance, and precipitation hardenability of some magnesium alloys (El Mahallawy *et al.*, 2017; Decker *et al.*, 2019). Zirconium is used in Mg alloys for grain refinement; it is currently the well-known element that has potent grain refining effects on the Mg-Zn alloys (Wang *et al.*, 2014; Karakulak, 2019). The microstructural behaviour of Zr grain refinement is poorly understood, but is believed to be caused by the crystal structure modification, intermetallic phases and lattice parameter similarity of Mg and Zr (Buzolin *et al.*, 2015; El Mahallawy *et al.*, 2017; Karakulak, 2019). It has been reported that Zr provides a strong grain refining effect by providing nucleation in Mg alloys not alloyed with Al. During the solidification of α-Mg, dissoluted atoms are rejected in the melt

and then separated on the edge of the growing dendrites, forming a constitutional super-cooling (CS) zone. Thermal gradient and elemental composition separation occurring just in front of the supercooling line allows the a-Mg phase to be limited without allowing grain swelling, at the same time, it increases the nucleation potential of a-Mg and provides a finer grain microstructure formation (Li *et al.*, 2007; Karakulak, 2019). Much attention has been paid to the fact that the addition of Zr to Mg-Zn-Zr series provide a pronounced grain refining effect and mechanical properties can be enhanced (Vinogradov *et al.*, 2012). Technically, the thermal solidification analysis is obtained from cooling curve of molten metal and/or a derivative of this curve. Characteristic peaks in the cooling curve are regarded as a regression relation between grain size and quality indices; ultimately the eutectic structure is used to evaluate the technical properties such as melt quality (Dobrzański *et al.*, 2009). By means of thermal cooling curves during the solidification period of the alloys; the composition, latent heat of crystallization (Ren *et al.*, 2011; El Mahallawy *et al.*, 2017), solid-liquid fraction, dendrite arm size, liquid-solid phase transition temperature, and eutectic transformation and intermetallic phases, characteristic temperatures are obtained (Dobrzański *et al.*, 2009). With the thermal analysis technique, the temperature changes in the analysed metallic material are recorded from completely liquid to fully solidified phases which form a temperature curve graph as a function of time. A cooling curve shows the temperature at which the latent heat of crystallization is released. The latent heat release in multi-metal alloys changes the slope of the cooling curve used to define the properties of transitions and phase transformations during crystallization. (Snopiński *et al.*, 2018). Although there are studies in the literature about the thermal analysis of Mg alloys, there is not much information about the cooling curve, intermetallics, phase transformations, grain size and latent heat which will be caused by different molds and different heat transfer effect of Zr concentration (Barber, 2004; Dobrzański *et al.*, 2009). A better understanding of the effect of nucleating elements such as Zr added to Mg alloys on solidification is crucial to understand their applicability to structural applications. It is known that as a result of solidification, the microstructure and phases formed depending on the cooling rate of the molds having different mold heat transfer coefficients vary. Therefore, both the effect of Zr and the microstructure, phase structure and wear behavior of the alloys cast into different molds were investigated. The wear properties of magnesium alloys are particularly important when applied to critical automobile parts such as air intake, transmission or suspension system (Godzierz *et al.*, 2019). This study indicates the influence of Zr concentration, and cooling rate on nucleation, microstructure, and mechanical properties of Mg-4Zn-(x)Zr (X= 0, 0.5, 1.0, 1.5, 2.0, 4.0 wt.% Zr) magnesium alloys. Also, this paper presents a Thermal Analysis (TA) study to determine phase transformation temperatures based on first, second derivative of cooling rates. Moreover, Mg-4Zn-(x)Zr alloys haven't been used for high-performance applications due to their low-hardness and wear resistance. In this work, the effects of adding zirconium on the wear resistance of Mg-4Zn-(x)Zr alloys were investigated to develop a modified type low-cost magnesium alloys with good performance. Furthermore, in this paper, the effect of dry wearing on surface hardness of Mg-4Zn-(x)Zr alloys that produced by a graphite mold and shell mold casting is explored under dry wearing condition.

## 2. MATERIALS AND METHODS

The pure Mg and Zn metals pieces were heated and melted in a graphite crucible, using induction heating. Continuous flow of $CO_2$ + 4% $SF_6$ mixed gas was used as protective covering gas, during the melting and casting. The melt temperature was kept at roughly 800 ºC and no grain modifiers were used. Zr was added in the form of Mg - 30 wt% Zr master alloy. The Zr quantity in Mg-4Zn alloy was increased from 0 Zr to 4 wt% Zr. and the chemical composition of specimens was shown in Table 1. Using a SiC impeller the melt was mixed and homogenized. In order to prevent the iron contamination, stem from steel impeller, SiC impeller was preferred because of its high melting temperature. Melt alloys are poured into a graphite mold and ceramic-based shell molds to reveal the effect of different cooling rates. During the

**Table 1.** The specific compositions of Mg-4Zn-(x)Zr alloys that cast into graphite and shell mold

| Alloy (Graphite Mold=GM) | Zn | Zr | Mg | Alloy (Shell Mold=SM) | Zn | Zr | Mg |
|---|---|---|---|---|---|---|---|
| Mg-4Zn (GM) | 4 | - | 96 | Mg-4Zn (SM) | 4 | - | 96 |
| Mg-4Zn-0.5Zr (GM) | 4 | 0.5 | 95.5 | Mg-4Zn-0.5Zr (SM) | 4 | 0.5 | 95.5 |
| Mg-4Zn-1Zr (GM) | 4 | 1 | 95 | Mg-4Zn-1Zr (SM) | 4 | 1 | 95 |
| Mg-4Zn-1.5Zr (GM) | 4 | 1.5 | 94.5 | Mg-4ZN-1.5Zr (SM) | 4 | 1.5 | 94.5 |
| Mg-4Zn-2Zr (GM) | 4 | 2 | 94 | Mg-4Zn-2Zr (SM) | 4 | 2 | 94 |
| Mg-4Zn-4Zr (GM) | 4 | 4 | 92 | Mg-4Zn-4Zr (SM) | 4 | 4 | 92 |

casting, continuous cooling data was collected from the castings made in graphite and shell mold by placing K-type thermocouples on the mold wall and in the liquid metal. All temperature-time data from liquid state to the end of solidification were collected by the Picolog data acquisition system in the millisecond sensitivity range. The cast magnesium alloys are removed from the molds after solidification, and macro examination is done and then prepared for metallographic examination. For metallographic inspection, the samples were cut and sanded with standard abrasive paper and polished with 0.5 μm alumina solution then immediately etched with 5 g of picric acid, 100 ml of ethanol and 15 ml of pure water.

The microstructures of the investigated alloys were observed using an optical microscope (OM, Nikon Eclipse L150), scanning electron microscope (SEM, Tescan-Mira3) with energy dispersive spectroscopy (EDS). The crystalline structures of α Mg, MgZn, and MgZr phases were characterized by X-Ray Diffraction (XRD, Rigaku D/MAX2500PC) using Cu Kα radiation. The detection was performed a step of 0.02° with a scanning speed of 1.2° $min^{-1}$. Tensile testing was performed by the Shimadzu/Trapezium with a speed of 5 mm/min at room temperature and hot temperature at 180 ºC, laboratory air/argon environment. The tensile test specimens were machined by CNC milling using the cast specimens. The gauge length of the tensile specimen was 60 mm, 14.5 mm in width and 6 mm in thickness. Brinell hardness tests were performed on both graphite and shell mold castings by applying 62.5 kg load.

Sliding wear tests were conducted in pin-on-disc wear testing against carburized and hardened AISI 8620 steel disc. Steel disc hardness was measured at 62 HRC. The pin-on-disc test specimens (Mg-4Zn-xZr alloys) were 20 mm in length and 6 mm in diameter. The pin surfaces were ground using 600 grit SiC paper then cleaned prior to each test. The rate of wear was a measure of weight loss in the samples, and a sliding velocity and volume loss per applied load. The wear rate as a function of pressure at 1000 m slip distance was calculated. In the wear tests, a pressure between 10 N and 30 N was applied on the pin. Especially when a new alloy is developed, the Pin-On-Disc method is used very often to measure the wear resistance of the alloy. For this reason, the pin-on-disc method was preferred in this study. In addition, the pin-on-disc method erodes a large surface area and this large area represents the entire sample independent of local errors. The pin-shaped specimen wearing surface area in this study was calculated as 28.27 $mm^2$.

## 3. RESULTS

For the measurement of grain size of alloys, grain counting was performed with software support by applying a standard linear intersection method to images at different magnifications taken with an optical microscope. The optical microstructure measurement revealed that the grain size reduces as the Zr content increases for each of the alloys (Fig.1). According to the analysis results, the largest grain size was found to be characteristic for Mg-4Zn (SM: Shell Mold) alloy.

As can be seen that the microstructure of the Mg-4Zn alloy predominantly consists of the α-Mg matrix in the casting state and the secondary phase is distributed in the grain boundaries as a secondary phase structure. A significant grain refining effect was achieved by adding Zr to the Mg-4Zn alloy as a nucleate. Grain size decreased from 186 μm to 40 μm in graphite mold alloys and from 333 μm to 60 μm in shell mold alloys. Depending on the amount to which Zr element is added, grain refining effect is shown in Table 2. As can be seen from Table 2, Zr addition can only make grain refining up to a limit value. Increasing the cooling rate, which is a second method for grain refining, is very important. A second noticeable difference in grain size results from the cooling rate of the graphite and shell mold. It took place in different cooling gradients in graphite mold and shell mold. In the graphite mold casting, faster solidification took place, resulting in a finer-grained microstructure.

**Table 2.** Average grain size of graphite and shell mold casting of Mg-4Zn-(x)Zr alloys

| Alloy | Graphite Mold (μm) | Shell Mold (μm) |
|---|---|---|
| Mg-4Zn | 186.36 | 343.07 |
| Mg-4Zn-0.5Zr | 166.66 | 180.95 |
| Mg-4Zn-1Zr | 97.95 | 134.61 |
| Mg-4Zn-1.5Zr | 91.55 | 131.11 |
| Mg-4Zn-2Zr | 86.75 | 75.02 |
| Mg-4Zn-4Zr | 40.61 | 60.1 |

**Table 3.** The HRB hardness of Mg-4Zn-(x)Zr alloys cast in graphite and shell mold

| Alloy | Graphite Mold (HRB) | Shell Mold (HRB) |
|---|---|---|
| Mg-4Zn | 72.8 | 62.9 |
| Mg-4Zn-0,5Zr | 73.2 | 66 |
| Mg-4Zn-1Zr | 81.7 | 74.9 |
| Mg-4Zn-1,5Zr | 78.2 | 77.2 |
| Mg-4Zn-2Zr | 78.1 | 80.5 |
| Mg-4Zn-4Zr | 87.6 | 85.6 |

Table 3 summarizes the hardness properties of the as-cast Mg–4Zn-xZr alloys that cast in GM and SM. Compared to Mg-4Zn, the hardness of Mg–4Zn alloys increased with the increase of Zr content until 1 wt% Zr. On the contrary, more Zr addition gives rise to deteriorated tensile strength. As can

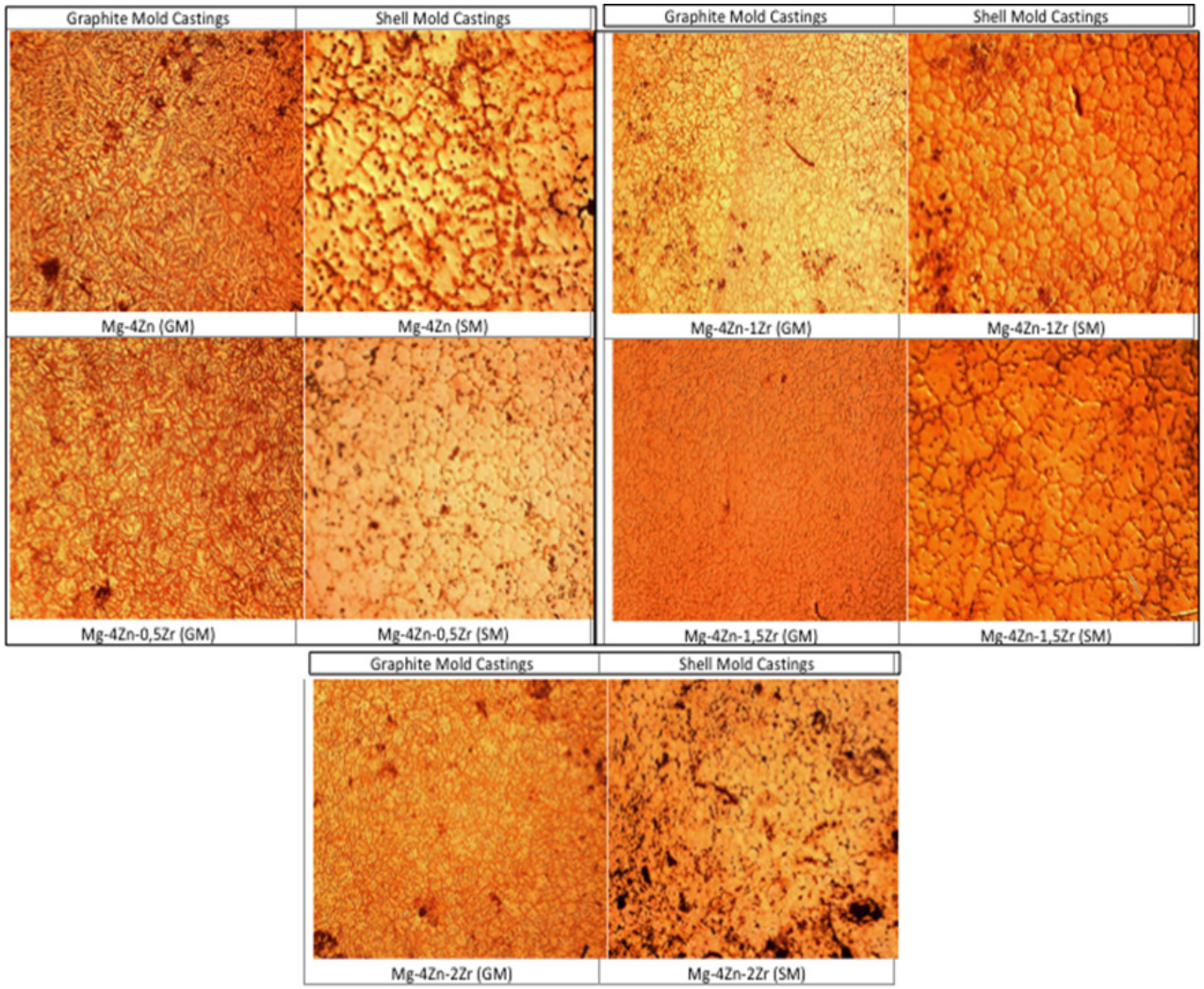


**Figure 1.** Optical microstructures of the as-cast Mg–4Zn alloys with different amount of Zr additions and different type of mold materials.

be seen in Table 4 the elongation of Mg–4Zn-1Zr alloy exhibits the maximum value as high as 4.9%. The UTS (Ultimate Tensile Strength) of Mg–4Zn was improved by from 81 MPa to 138 MPa due to the addition of 1 wt.% Zr. As a result, Mg-4Zn-1Zr (GM) alloy exhibits the best mechanical property.

## 4. DISCUSSION

One of the main objectives of this study is to measure the synergistic effect of grain refiner methods resulting from the cooling-solidification rate of alloys and obtained with the addition of alloy elements. The reason for adding alloy elements to the melt is that the alloy elements with limited solubility in the solidifying grains are enriched at the solid / liquid interface. This enrichment of dissolved atoms at the solid / liquid interface restricts the growth of nucleated particles. Solid protrusions that try to grow dendritically in certain planes show excessive roughening with the effect of alloying elements. Different alloy elements have different restriction ability. This situation arises from different features such as "solubility, atomic radius, valence value" (Karakulak, 2019). Reduced grain size results in increased mechanical properties such as higher tensile / compressive strength, ductility, hardness, and tribological properties such as wear resistance (Wu *et al.*, 2012; Li *et al.*, 2015). Cao et al. indicated an effective grain refining property of zinc added to magnesium by 2% by weight or more (Cao *et al.*, 2005). Although Zn added to magnesium over 2% by weight does not affect grain refining measurements much, Zn above 2% causes increase in strength by providing new phases with Mg. At 350 °C, Zn has a 6.2wt% solubility in Mg. As the temperature decreases towards the room temperature, the solubility of Zn decreases and forms the $Mg_7Zn_3$ phases (Kapinos *et al.*, 2014). The increase in hardness is associated with densification level, grain refining and homogeneously precip-

**Table 4.** Tensile test results of Mg-4Zn-xZr alloys. Tensile test results of Mg-4Zn-xZr graphite mold cast alloys

| Alloy (GM) | % Elongation | Tensile Strength (MPa) | Hot Tensile (MPa) |
|---|---|---|---|
| Mg-4Zn | 2.55 | 81.29 | 50 |
| Mg-4Zn-0,5Zr | 4.33 | 116.28 | 88 |
| Mg-4Zn-1Zr | 4.9 | 138.64 | 92 |
| Mg-4ZN-1,5Zr | 3.8 | 115.67 | 94 |
| Mg-4Zn-2Zr | 2.4 | 120.89 | 98 |
| Mg-4Zn-4Zr | 1.57 | 120.51 | 81 |
| **Tensile test results of Mg-4Zn-xZr shell mold cast alloys** | | | |
| **Alloy (GM)** | **% Elongation** | **Tensile Strength (MPa)** | **Hot Tensile (MPa)** |
| Mg-4Zn | 2.73 | 79.6 | 45 |
| Mg-4Zn-0,5Zr | 4.41 | 112.5 | 76 |
| Mg-4Zn-1Zr | 4.79 | 131.34 | 81 |
| Mg-4ZN-1,5Zr | 3.68 | 112.88 | 83 |
| Mg-4Zn-2Zr | 2.24 | 118.63 | 86 |
| Mg-4Zn-4Zr | 2.01 | 110.52 | 78 |

itated $Mg_7Zn_3$ phase. The homogeneously dispersed $Mg_7Zn_3$ phase with higher hardness can serve as a reinforcing phase by preventing dislocation movement between grains. In addition, the Zn solid solution formed in α-Mg supports the increase in hardness. Based on the solid solution strengthening theory of Mg alloys, the lattice distortion caused by the solid solution of Zn limits the dislocation movement between the grains and boundaries (Shuai *et al.*, 2017; Zhang *et al.*, 2018).

Zirconium is used as the most common grain refiner in Mg alloys that not contain Al, Mn, Si, Fe, Sn, Ni, Co and Sb (Ali *et al.*, 2015). The increase in tensile strength until 1 wt% Zr and 1.5 wt% Zr can be explained by Hall–Patch relationship. According to the Hall-Petch law, which explains the relationship between grain size and yield strength, strengthening by grain refinement in magnesium alloys is highly effective due to high K coefficient (Cai *et al.*, 2012; El Mahallawy *et al.*, 2017).

The microstructure of the alloys added with 1% and 1.5% Zr is in the form of cellular matrix, and Mg-4Zn and Mg-4Zn-0.5Zr form a more obvious dendritic structure (Buzolin *et al.*, 2015; Li *et al.*, 2007). The Mg-4Zn-2Zr and Mg-4Zn-4Zr alloys exhibit a heterogeneous microstructure with grain boundaries surrounded by Zn and Zr intermetallic phases and semi-continuous diffused rejected phases (Li *et al.*, 2007). In Mg-Zn-xZr alloys, the main strengthening phase is reported to be $Mg_7Zn_3$, $MgZn_2$ and MgZn (Yuan *et al.*, 2019). In this study, similar strengthening phases were formed. These phases are likely to increase mechanical properties and wear resistance. The amount of microporosity due to the increasing Zr ratio, and semi-continuous phases are the main factors in the decrease of mechanical properties.

Mg-4Zn castings without Zr addition for graphite and shell mold show strong dendritic structure and coarse grains and Mg-Zn, $Mg_7Zn_3$ spheres having a very bright contrast (Fig 2). When the microstructure of the graphite die-cast alloy is examined, the α-Mg matrix is usually formed and the MgZn intermetallic is observed. When the microstructure of the shell-cast alloy is examined, it is usually formed as the main matrix of α-Mg and $Mg_7Zn_3$ intermetallic is observed. Fig. 2b at higher magnifications (Circle) reveals that the intermetallic Mg–Zn particles in alpha magnesium matrix and $MgZn_2$ eutectic phase which is distributed along the a-Mg boundaries. Spherical Mg-Zn micro-particles are much smaller and gathered in the Mg-4Zn alloys comparing the Zr added alloys (Vinogradov *et al.*, 2012). Also average diameter of Mg-Zn spheres in Mg-4Zn (GM) was measured approximately 5 mm and Mg-4Zn (SM) was 9 mm. When the microstructure of the graphite die-cast Mg-4Zn-0.5Zr alloy is examined, the matrix of α-Mg is generally formed and the MgZn and MgZr intermetallic are observed. When the microstructure of the shell-cast Mg-4Zn-0.5Zr alloy is examined, the matrix of α-Mg is generally formed and the $Mg_2Zn$ and MgZr intermetallic are observed. Furthermore, as can be seen in Fig. 3, the addition of Zirconium obviously reduces the grain size of Mg-4Zn alloy. MgZn and MgZr intermetallic were observed in the microstructure of the Mg-4Zn-0.5Zr alloy cast graphite die-cast in the grain boundaries of the α-Mg matrix. In the microstructure of the shell-cast Mg-4Zn-0.5Zr alloy, $Mg_2Zn$ and MgZr intermetallic were observed with the

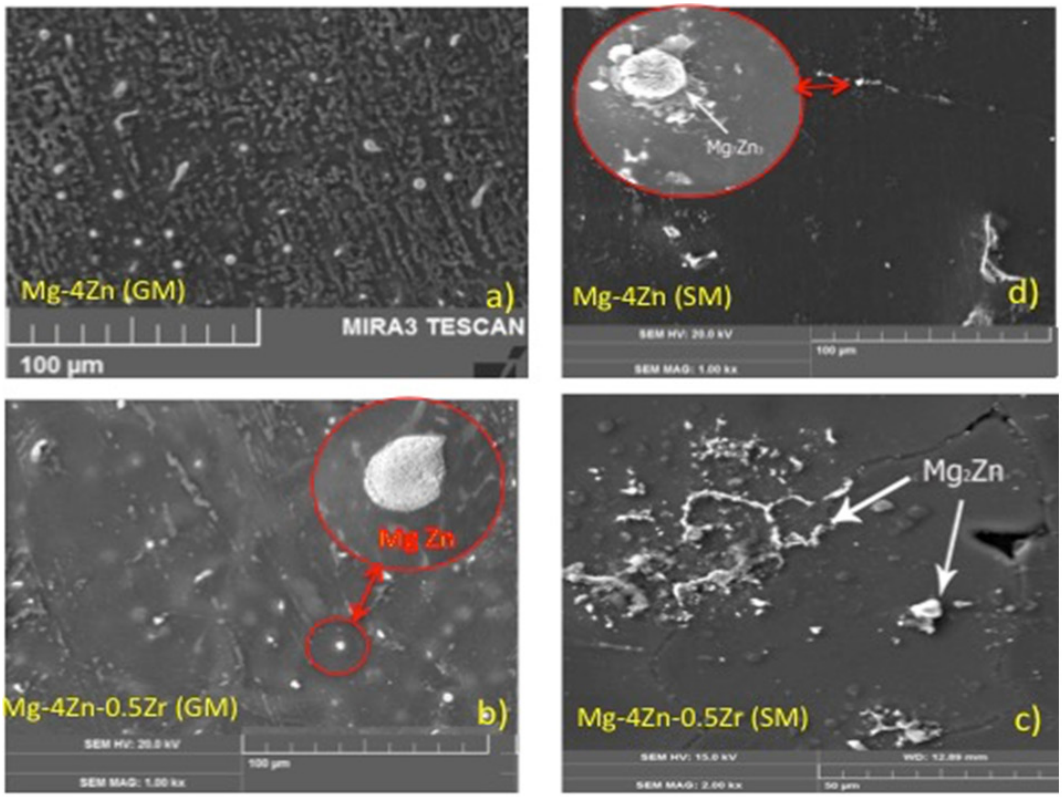


**Figure 2**. SEM images and related phases of: a) Mg-4Zn Graphite mold (GM) casting, b) Mg-4Zn Shell mold (SM) casting, c) Mg-4Zn-0.5Zr (GM), and d) Mg-4Zn-0.5Zr SM.

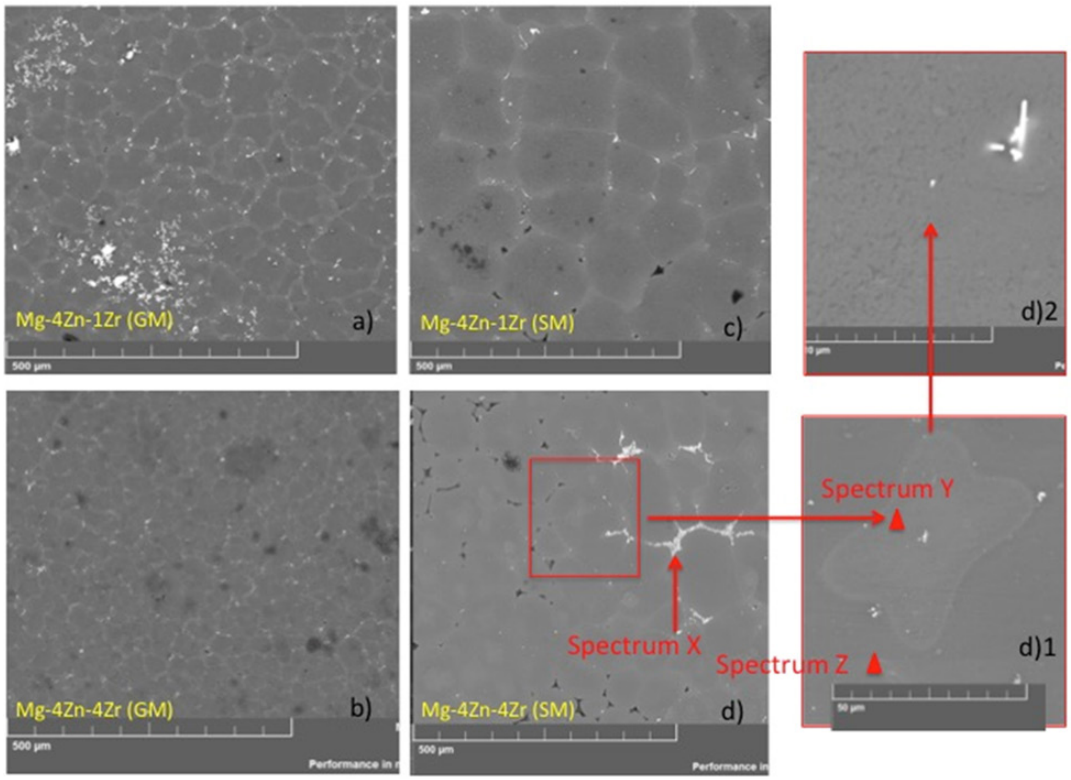


**Figure 3**. SEM images and related phases of: a) Mg-4Zn-1Zr (GM), b) Mg-4Zn-4Zr (GM), c) Mg-4Zn-1Zr (SM), and d) Mg-4Zn-4Zr (SM), d1) 10X magnification of rectangle panel in Fig. d, d2) 5X Magnification of d1.

α-Mg matrix in general. According to the results of the EDS analyzes, α-Mg matrix and $Mg_{15}ZnZr_{18}$ intermetallic were observed in the microstructure of GM-cast Mg-4Zn-1Zr alloy (Fig 3). Similarly, based on the EDS at.% calculation, the α-Mg matrix and the $Mg_{17}Zn_6Zr_2$ intermetallic were found in the microstructure of the SM Mg-4Zn-1Zr alloy. In Fig 3. Spectrum the letter X shows the white irregular shape of boundary phase that mainly composed of Zr and Zn phase such 41.26%Mg, 15.33%Zn and 43.41%Zr. The spectrum Y was detected from a bone-like special shape in red rectangle shown in Fig 3d and Fig.3d1 consisting following spectroscopic results 92.63 wt.%Mg, 2.73 wt.%Zn, 4.65 wt%Zr. The bone-like shape or another shape of Zr based phases was located in the grains. The EDS spectra Z that measured out of the bone shape was 95.82 wt%Mg, 2.73 wt%Zn and 0.67 wt%Zr. This value is nearly solubility limits of Zr and Zn in Mg.

SEM-EDS examination results reveals that the microstructure of GM cast Mg-4Zn-1.5Zr alloy, mainly consist of α-Mg, MgZn and MgZr intermetallic; on the other hand, SM cast Mg-4Zn-1.5Zr alloy, has α-Mg, $Mg_2Zn$ and MgZr intermetallic. Similar phase and microstructure results were investigated for the 2 wt%Zr addition for each mold type. Drastically phase changing and grain size reducing effect was observed in the 4 wt%Zr addition samples that cast into SM. The new phase stoichiometry was calculated as $Mg_7ZnZr_2$.

Ren et al signify the effect of the second Mg-Zn-Zr based intermetallic phases on mechanical property, such as ZnZr, $Zn_2Zr_3$, $Zn_2Zr_3$+$Zn_2Zr$ etc. in cast Mg–Zn–Zr alloys (Ren *et al.*, 2011). It has been revealed that the zinc acts as grain refiner (Arroyave and Liu, 2005). When the size and distribution of stable Zn-Zr intermetallic compounds are well controlled, it can be expected that the strength of Mg alloys may increase. During the controlled solidification, Zn element in the Mg alloys goes into the solid solution in the α-Mg matrix, thereby increasing the matrix strength through solid solution strengthening (El Mahallawy *et al.*, 2017; He *et al.*, 2018).

When the graphite mold and shell mold casting method are compared, the cooling of the shell mold is slower and due to the fact that the diffusion process is also time-dependent, a more homogeneous microstructure was observed at the shell mold casting. In order to find out the microstructure, phase and thermal effects of Zr addition and mold type, thermal analysis was performed for each sample by using graphite and shell mold and temperature data acquisition system. The cooling curves of graphite and shell mold casting were given in Fig.4. To find

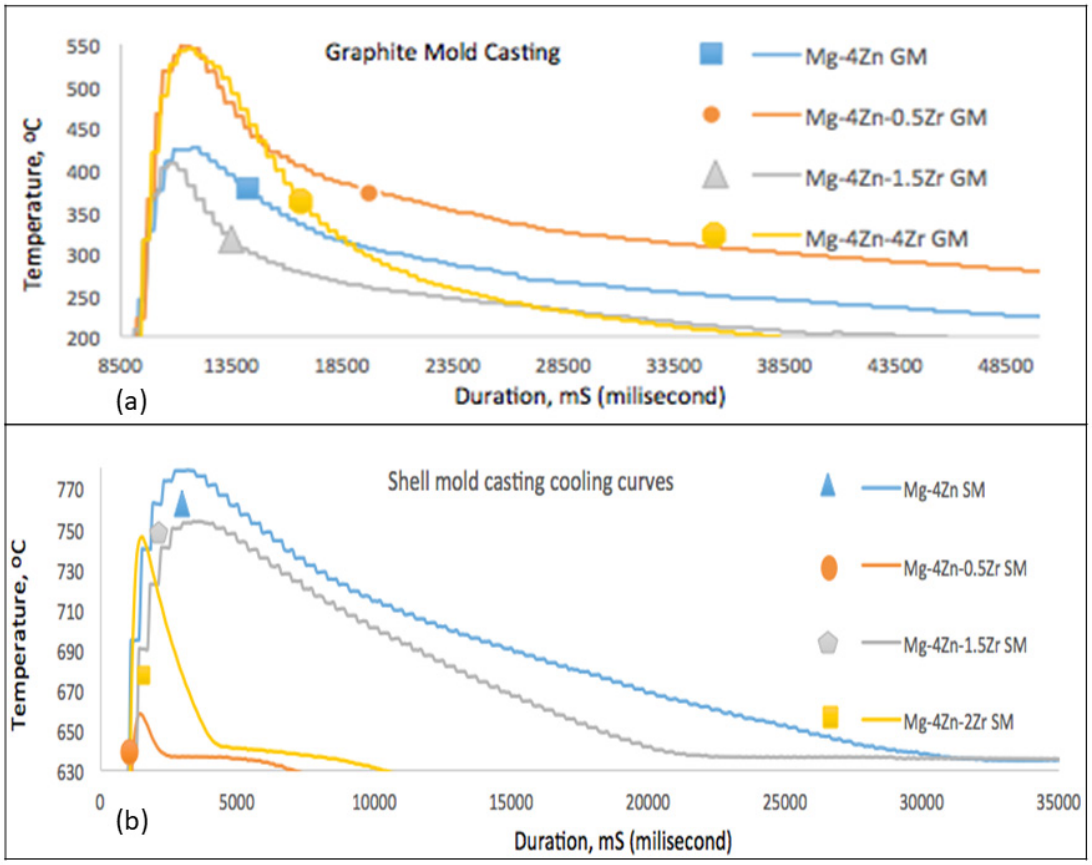


**Figure 4.** Thermal analysis curves of (a) graphite mold and (b) shell mold casting Mg-4Zn-xZr alloys.

out further investigation, first and second derivatives of cooling curves were also examined to fully understand the phase transformation and stored-released energy relations. Phase transformations can be detected in these cooling curves. Because these curves form peaks in the phase transformation temperatures, by examining these peaks, the transformation and types of the phases can be determined.

When the Mg-% 4Zn alloy was examined, MgZn intermetallic phase was observed. At higher ratios of Zn, in addition to α-Mg and MgZn, the intermetallic phase $Mg_{51}Zn_{20}$ was also detected by the first derivative of cooling curves. These phases are phases rejected from the Zn solid/liquid interface and accumulate at the triple intersections of the grain boundaries and along the grain boundary. The general shape of MgZn phase was observed as spherical and/ or elliptic geometry as shown in Fig. 2d.

Mg–Zn binary phase formation via a two-step transformation with the eutectic reaction, L →α (Mg) + β ($Mg_7Zn_3$), at 340 °C followed by the eutectoid reaction, β ($Mg_7Zn_3$) →α(Mg)+ γ(MgZn), at 312 °C is reported in the literature (Prabhu *et al.*, 2018). In the Mg-Zn-Zr ternary alloy, Zr can increase the β1′ phase stability and cause more stable Mg (Zn, Zr) instead of less stable $MgZn_2$. In the literature, the thermodynamics and kinetics of Mg-Zn and Mg-Zn-Zr alloys in the solidification and liquid-solid zones have been studied in detail. The thermodynamic interaction of Zr addition on $Mg_7Zn_3$, $MgZn_2$ and MgZn formations reveals that these compounds and solid solutions can be formed in both Mg-Zn and Zn-Zr binary systems. Zr atoms prefer to form clusters with Zr atoms instead of combining with Mg atoms in liquid Mg-Zr alloys. Due to the tendency of phase separation in Mg-Zr system, it decreases the possibility of Zr atoms to combine with Mg to form stable compounds (Dobrzański *et al.*, 2011; Yuan *et al.*, 2019).

The phase transformation temperatures obtained in Mg-4Zn shell die casting alloys are as follows: The first peak is the temperature of the liquid curve. The recorded temperature for this characteristic peak is 635 °C degrees. The temperature in the second peak region is 630 °C and MgZn intermetallic occurs at this temperature. The third peak temperature is 581 °C and it is possible to form $Mg_xZn_y$ eutectic phases at this temperature value. The fourth peak temperature is 431 °C that the α-Mg secondary phase forms.

The phase transformation temperatures observed in the Mg-4Zn graphite mold casting alloy are: Mg-Zn alloy is observed in the first peak region and the temperature is 271 °C. The temperature of the second peak is 206 °C. At this temperature MgZn intermetallic is formed.

The phase transformation temperatures obtained in Mg-4Zn-0.5Zr Shell mold are summarized below. The first peak at 637 °C is the temperature of the liquidus line. The temperature in the second peak is 630 °C. The temperature at the third peak is 584 °C and Mg-Zn intermetallic is observed at this temperature. The temperature in the fourth peak region is 484 °C and the α-Mg secondary phase forms (Prabhu *et al.*, 2018; Yuan e *et al.*, 2019).

The phase transformation temperatures obtained in the Mg-4Zn-0.5Zr graphite mold casting alloy are as follows. The temperature at the first peak is 320 °C and Mg-Zn alloy is formed at this temperature. The temperature in the second peak region is 258 °C. This region forms the α-Mg secondary phase. The temperature in the third peak region is 200 °C. MgZr-MgZn intermetallic formed.

The phase transformation temperatures obtained in the Mg-4Zn-1.5Zr Shell mold casting alloy are: The first peak is the liquid phase. The temperature here is 637 °C. The temperature at the second peak is 632° C. Here the Mg-Zr alloy is formed. The temperature at the third peak is 586 °C. Here MgZn intermetallic occurs. The temperature of the fourth peak area is 511 °C. Here MgZr intermetallic occurs.

The phase transformation temperatures obtained in the Mg-4Zn-1.5Zr (GM) are: The first peak area is 271 °C. Here the MgZn or MgZr intermetallic occurs. The second peak is at 204 °C. Here the Mg-Zn alloy is formed.

The phase transformation temperatures obtained in the Mg-4Zn-2Zr (SM) are: The region where the first peak is located. Here the temperature is 640 °C. The temperature in the second peak region is 613 °C. Here the MgZn alloy is formed. The temperature in the third peak region is 591 °C. Here MgZn intermetallic occurs. The temperature in the third peak area is 510 °C. Here MgZr intermetallic occurs.

The phase transformation temperatures obtained in the Mg-4Zn-2Zr (GM) are: The temperature in the first peak region is 291 °C. Here an Mg-Zn alloy is formed. The temperature in the second peak region is 207 °C. Here the Mg-Zn or Mg-Zr intermetallic occurs. The problem of gas and porosity was observed in the casting due to the decrease in fluidity and the high dissolution temperature in Mg-4Zn-4Zr alloy.

A cooling rate change from 0.03 °C/s (Mg-4Zn GM) to 0.048 °C/s (Mg-4Z-2Zr GM) causes the remarkable decrease of the grain size. An increase of the Zirconium mass concentration causes a slight decrease in the grain size and cooling rate. Similar results were observed for other alloys examined in this study. Sliding wear behavior of an Mg-4Zn-XZr graphite mold casting and shell mold casting has been examined under varying applied pressure, sliding speed and at a fixed sliding distance 1000 m. The effect of Zr addition and milling machining pressures on alloy wear resistance has been tested comparatively. Sliding wear tests were conducted in pin-on-disc wear testing against carburized steel disc.

The pin shape samples were 20 mm in length and 6 mm in diameter. The rate of wear was a measure of weight loss in the samples, and a sliding velocity and volume loss per applied load. The wear rate as a function of pressure at 1000 m slip distance is shown in Fig. 5 (a-b). As can be seen, the increased pressure level indicates that the wear rate increases in all samples. No transition pressure was detected. It is noted from the figure that the wear rate linearly increases. It may be noted that the wear rate of the Mg-4Zn-1Zr GM alloy is found to be lower than that of the graphite mold cast materials (Fig. 5a). The wear rate of the Mg-4Zn-1Zr SM and Mg-4Zn-0,5Zr SM alloy is found to be lower than that of the shell mold cast materials (Fig. 5b).

The wear rates observed in GM and SM castings at 30 N pressure applied on the sample are given in Fig. 5 (c, d) as a function of sliding speed. Initially the wear rate is increased up to a sliding speed of 0.7 $m \cdot s^{-1}$ and is decreased down to a sliding speed of 1 $m \cdot s^{-1}$. It clearly indicates that the wear rate is almost similar to sliding speed. Again, the optimum wear rate was achieved at the Mg-4Zn-1Zr GM alloy. The wear loss rate increases with the applied load in both of the graphite and shell mold castings. It has been observed that the wear rate increases linearly as a function of the pressure applied to the sliding wear. It is the fact that the hard particles that break up with the increase of the applied pressure penetrate the Mg-based soft pin surface and at the same time the softness and breakage increase (Godzierz *et al.*, 2019). The addition of Zr up to 1.5 wt% is found to enhance the wear properties. The lower wear rates of Zr added alloy can be attributed to the reinforcement intermetallic phase of MgZr, MgZn, ZnZr.

The SEM-BSE mode images indicate that both the abrasive and adhesive wear mechanisms have occurred on the worn surface of the alloys. Evidence of local small plastic deformation was found in the traces of wear, but the wear mechanism of the alloys did not change markedly with the addition of Zr. The SEM elemental analysis results also indicate the presence of element Oxygen with Mg, Zn, and Zr element. Frictional abrasive wear is formed in the form of deep grooves in the direction of friction, in the form of plastering, depending on the difference in hardness between the pin and the steel disc. The wear of 30 N loads is shown in the form of severe wear on the sample surfaces. Typical wear traces like broad grooves with a size of ~150-175 μm and oxidized areas and plastic deformation cracks was shown on the Mg-4Zn alloy surface using yellow arrows respectively (Fig. 6a). The smooth wear surface of Mg-4Zn-0.5Zr alloys few shallow grooves and oxides (Fig. 6b). Figure 6 indicate that both abrasive and adhesion mechanism were detected on the wear traces of the samples. Mandal *et al.* (2019); carried out abrasion tests by adding Pb, Sn and Zr elements to Mg-Al-Zn alloy. They observed that wear losses increased proportionally due to increased load as a result of wear tests. They proposed a similar volumetric loss mechanics as wear mechanism (Mandal *et al.*, 2019).

The effect of alloying element (Zr) on the wear rate and the friction coefficient shows that the wear

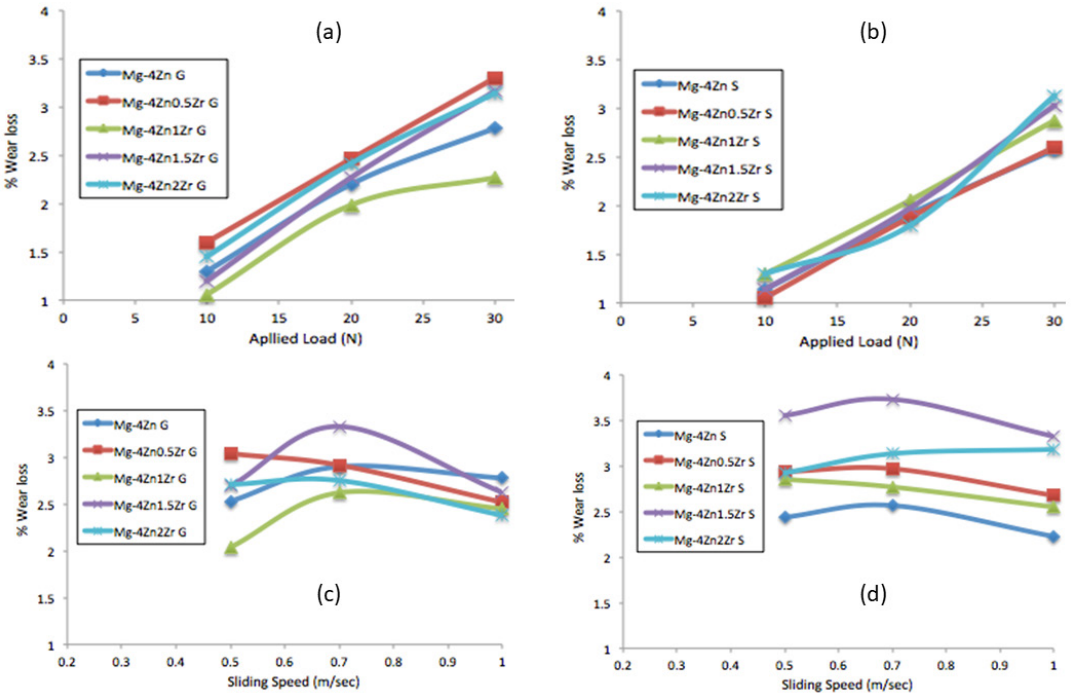


**Figure 5.** Effect of (a) applied load on wear loss of graphite mold cast, (b) Wear loss of shell mold cast as a function of applied load, (c) Wear loss of graphite mold cast as the function of sliding speed, and (d) Wear loss of shell mold cast as a function of sliding speed.

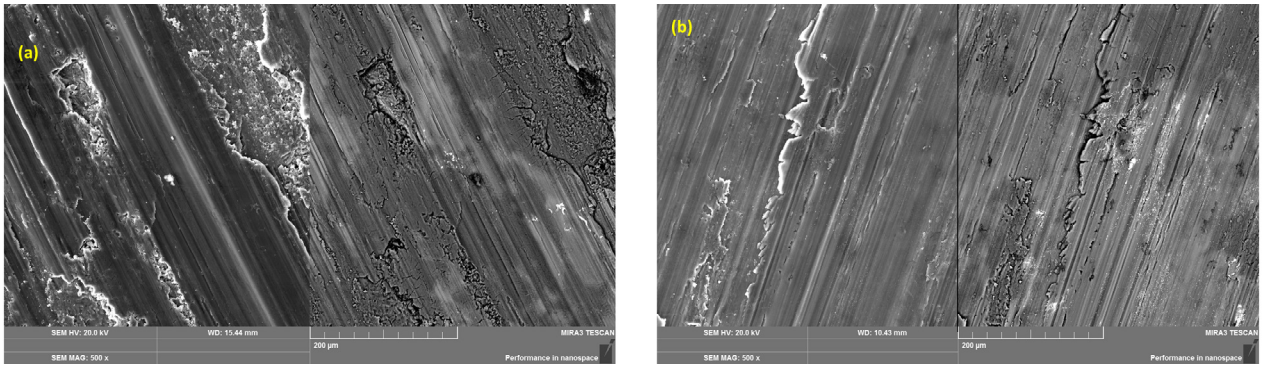


**Figure 6.** SEM micrographs of the worn surfaces of the a) Mg-4Zn SM casting and b) Mg-4Zn-0.5Zr SM casting after 1000 m sliding distance under 30 N.

**Table 5.** Dry sliding wear test results of Mg-4Zn-(x)Zr Graphite Mold and Shell Mold cast alloys

| **Alloy (GM)** Graphite Mold Cast | **Sliding** Distance (m) | **Aplied Load 10 N** Wear rate $mm^3/mm/1000$ | **Aplied Load 20 N** Wear rate $mm^3/mm/1000$ | **Aplied Load 30 N** Wear rate $mm^3/mm/1000$ |
|---|---|---|---|---|
| Mg-4Zn | 1000 | 4.79 | 4.87 | 5.13 |
| Mg-4Zn-0.5Zr | 1000 | 4.3 | 4.39 | 4.74 |
| Mg-4Zn-1Zr | 1000 | 4.1 | 4.28 | 4.72 |
| Mg-4ZN-1.5Zr | 1000 | 4.05 | 4.19 | 4.58 |
| Mg-4Zn-2Zr | 1000 | 4.28 | 4.35 | 4.67 |
| Mg-4Zn-4Zr | 1000 | 4.12 | 4.26 | 4.59 |
| **Alloy (SM)** Shell Mold Cast | **Sliding** Distance (m) | **Aplied Load 10 N** Wear rate $mm^3/mm/1000$ | **Aplied Load 20 N** Wear rate $mm^3/mm/1000$ | **Aplied Load 30 N** Wear rate $mm^3/mm/1000$ |
| Mg-4Zn | 1000 | 4.89 | 4.92 | 5.28 |
| Mg-4Zn-0.5Zr | 1000 | 4.65 | 4.69 | 5.15 |
| Mg-4Zn-1Zr | 1000 | 4.59 | 4.61 | 5.12 |
| Mg-4ZN-1.5Zr | 1000 | 4.49 | 4.78 | 4.98 |
| Mg-4Zn-2Zr | 1000 | 4.57 | 4.63 | 4.86 |
| Mg-4Zn-4Zr | 1000 | 4.45 | 4.64 | 4.97 |

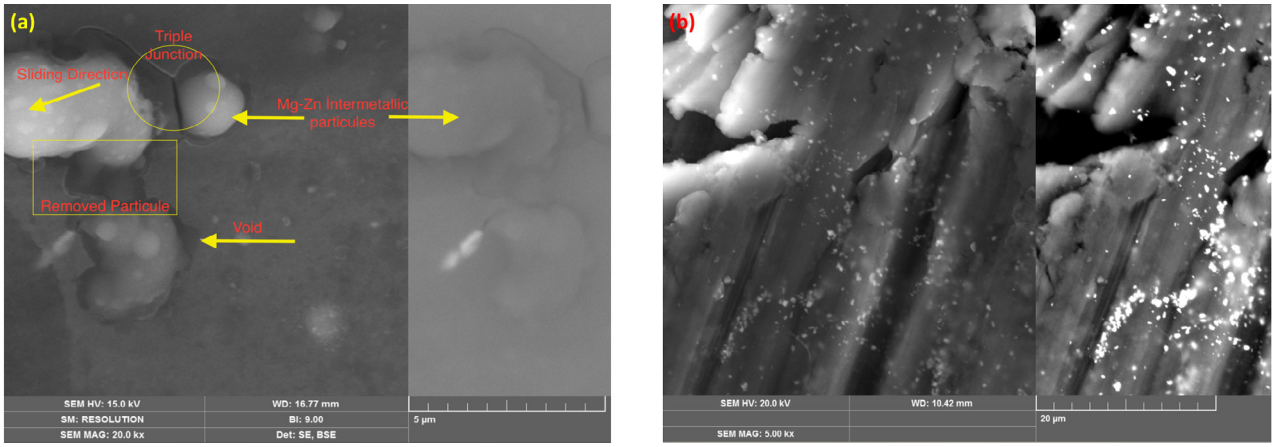


**Figure 7.** SEM details of the worn surfaces of the a) Mg-4Zn GM casting and b) Mg-4Zn-0,5Zr SM casting after 1000 m sliding distance under 30 N.

rate of alloy Mg-4Zn GM and SM remarkably decreased with increasing Zr up to 1.5 wt%Zr. The increase in wear resistance with the addition of Zr has been observed as the resistance of the fine-grained structure to plastic deformation, and is also the wear resistance of the Zr-based intermetallic phases formed. The wear rate then remains at relatively low and constant values with the addition of more than 2 wt%Zr. This behavior is also observed in graphite and shell die casting alloys (Table 5). This is because excess Zr-saturated intermetallics delaminate from the wear line in blocks and rupture into large debris. SEM analyses showed that both MgZn spherical intermetallic have good adherence with the Mg matrix, but after a certain sliding distance the adhesion mechanism and particle debonding observed on the worn surface of the alloys (Fig. 7a). It is believed that the discrete Mg Zn eutectic structure and the homogeneously dispersed Mg Zr phase are the main factors in reducing the wear rate as seen in Fig. 7a MgZn spherical particles increase the load-bearing capacity of matrix. On the other hand, increasing the Zr content mainly contains continuous and brittle MgZr intermetallic at the grain boundary and in the grains. During the wear of the Fig 7b, the intermetallic phases were removed from the surface then behaved abrasive wear debris at the interface. However, the debris that worn from the surface was imbedded in the matrix which cause no weight loss. In order to examine the more severe conditions of wear, both the sliding speed and the applied load have been gradually increased, the debris of all Mg-4Zn alloys shows two types of characteristic agglomerates, in the form of small particles and relatively large laminate debris. The high magnification images of the small particle debris are shown in Fig. 7b. It consists of fractured MgZr particles, as shown in Fig. 7b. As a general acceptance, the wear rate is strongly dependent on the hardness of the alloys. In fact, in the work, the hardness of the main alloy increased with increasing added Zr element.

Figure 8 shows the Sem-Map image of Mg-4Zn-2Zr alloy and the related stable intermetallic phases during the hot tensile test. The high temperature stable phases prevent the grain boundry slip and increases the hot tensile strength. Fig. 9 shows the XRD patterns of Mg-4Zn and 1 wt%Zr, 2 wt%Zr added alloys. XRD result shows that the alloy was composed of Mg, MgZn and MgZr phases, as indicated in Fig. 9. In the alloys with both different casts (Shell and Graphite) and Zr not added, two peaks around (2θ) 80 degrees were observed, but as the amount of Zr added increased, these peaks became more prominent. In addition, new formation peaks were also detected at (2θ) 70 degrees. Since the Zr content is too low, the XRD detected the strongest peak of Mg and Mg-Zn-Zr phases. However, in the Mg-Zn-Zr alloy, three peaks were observed at two-theta 57, 63.5 and 78.5.

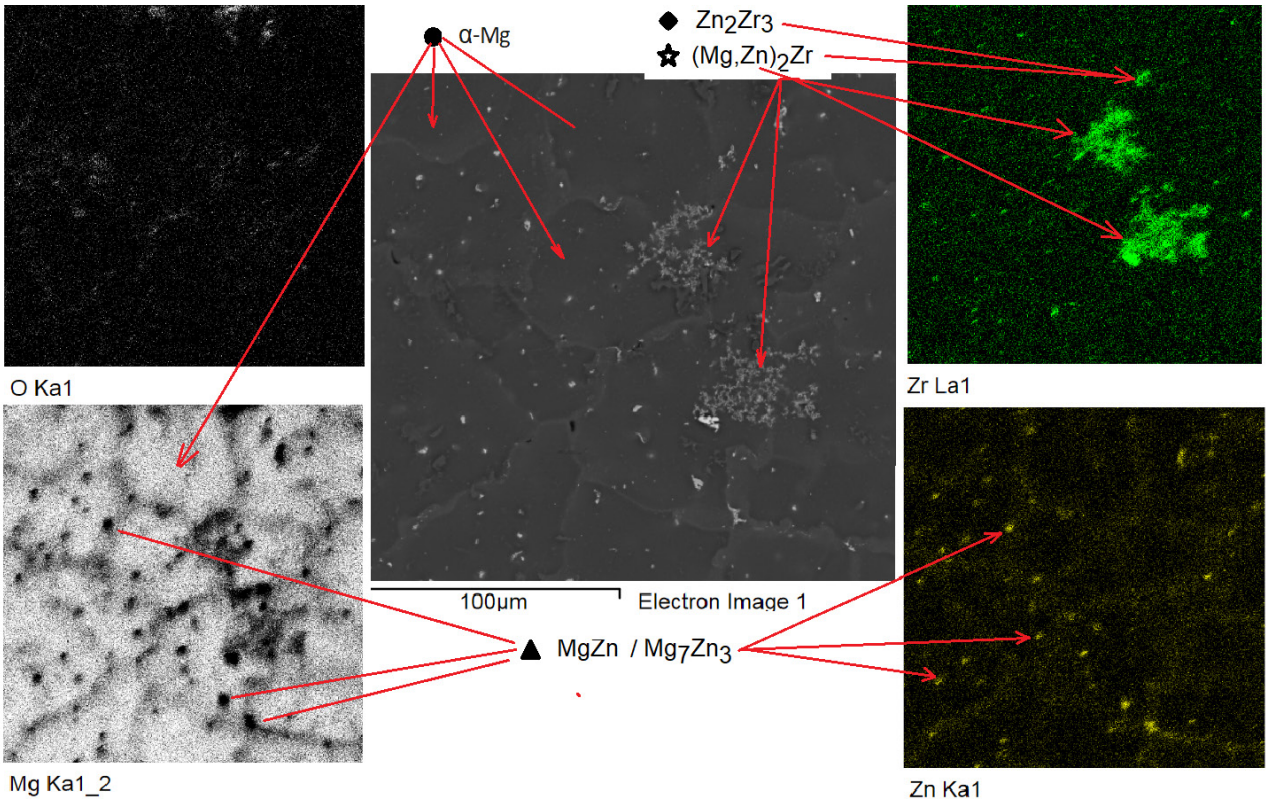


**Figure 8.** SEM-MAP analysis of Mg-4Zn-(2)Zr alloys (GM).

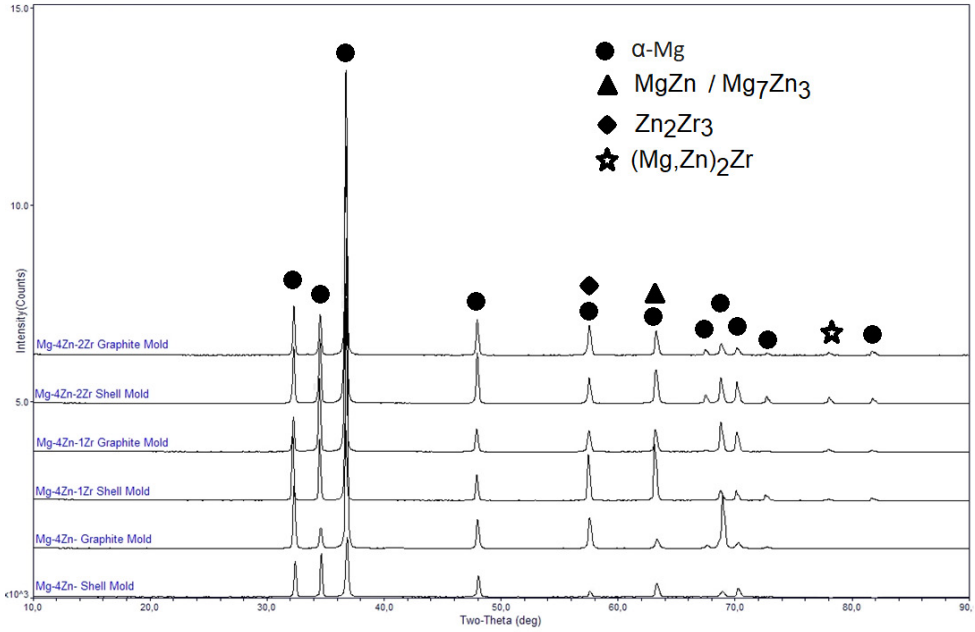


**Figure 9.** XRD pattern of Mg4Zn and Mg-4Zn-XZr alloys.

## 5. CONCLUSIONS

Fine grain microstructure can be obtained by increasing the cooling rate in thin section castings, but thick sections are not possible. In this study, the synergistic effect of grain refining techniques has been studied both by increasing the cooling rate with graphite mold and adding Zr. It has been revealed that Zr added to the Mg-4Zn alloy, which is both cast into the graphite mold and the shell mold, has a pronounced grain refining effect.

The microstructures of the as-cast Mg4Zn alloy are composed of the grain boundary Zn and the microstructures of the as-cast Mg4Zn-1Zr and 2Zr alloy are composed of the grain boundary ZnZr, MgZn, MgZr and Zr rich-phase and the α-Mg phase. The solubility of Zr in the liquid phase decreased significantly and proportionally to the drop in temperature and caused the formation of high density Zr and / or Zr rich nucleus due to supercooling. The hardness of both casting alloys increased with the addition of Zr up to 2% by weight. Zr addition up to 1 wt% increased the UTS of the alloys. The maximum tensile strength was achieved on the Mg-4Zn-1Zr the elongation was 4.9 wt% and the tensile strength was 138.64 MPa.

It was understood that the rate of wear increased with the increase of pressure applied. However, the wear resistance of the alloy has been observed to improve significantly with the addition of Zr. The Zr added alloys exhibited a lower wear rate than that of the Mg-4Zn alloy. The wear resistance of the Mg-4Zn-1Zr alloy poured into the graphite mold increased with intermetallic phases formed and a small amount of grain refining effect. No apparent effect was observed in the castings of the shell mold. The wear resistance of the Mg-4Zn-2Zr alloy increases the cumulative volume loss with an increased applied load. Considering basic wear mechanisms, oxidative wear and delamination wear characteristics due to high load have been observed.

## REFERENCES

Ali, Y., Qiu, D., Jiang, B., Pan, F., Zhang, M.-X. (2015). Current research progress in grain refinement of cast magnesium alloys: A review article. *J. Alloys Compd.* 619, 639–651. https://doi.org/10.1016/j.jallcom.2014.09.061.

Arroyave, R., Liu, Z.K. (2005). *Thermodynamics of Mg-Zn-Zr: Implication on the effect of Zr on grain refining of Mg-Zn alloys. In Magnesium Technology*. TMS Annual Meeting, San Francisco, CA, USA, pp. 203-208.

Barber, L.P. (2004). Characterization of the Solidification Behavior and Resultant Microstructures of Mg-Al Alloys. A Thesis of Master, Worcester Polytechnic Institute, pp. 10-46.

Bazhenov, V.E., Koltygin, A.V., Sung, M.C., Park, S.H., Titov, A.Y., Bautin, V.A., Matveev, S.V., Belov, M.V., Belov, V.D., Malyutin, K.V. (2020). Design of Mg-Zn-Si-Ca casting magnesium alloy with high thermal conductivity. *J. Magnes. Alloy* 8 (1), 184–191. https://doi.org/10.1016/j.jma.2019.11.008.

Buzolin, R.H., Tolnai, D., Mendis, C.L., Stark, A., Schell, N., Pinto, H., Kainer, K.U., Hort, N. (2015). *Investigation of compression behavior of Mg-4Zn-2(Nd,Gd)-0.5Zr at 350 °C by in itu Synchrotron Radiation Diffraction*. In *Magnesium Technology.* TMS, pp. 103-107. https://doi.org/10.1007/978-3-319-48185-2_21.

Cai, S., Lei, T., Li, N., Feng, F. (2012). Effects of Zn on microstructure, mechanical properties and corrosion behavior of Mg–Zn alloys. *Mater. Sci. Eng. C* 32 (8), 2570–2577. https://doi.org/10.1016/j.msec.2012.07.042.

Cao, P., Qian, M., StJohn, D.H. (2005). Native grain refinement of magnesium alloys. *Scripta Mater.* 53 (7), 841–844. https://doi.org/10.1016/j.scriptamat.2005.06.010.

Chalisgaonkar, R. (2020). Insight in applications, manufacturing and corrosion behaviour of magnesium and its alloys – A review. *Mater. Today Proc.* 26 (2), 1060-1071. https://doi.org/10.1016/j.matpr.2020.02.211.

Dadić, Z., Živković, D., Čatipović, N., Marinić-Kragić, I. (2019). Influence of steel preheat temperature and molten casting alloy AlSi9Cu3(Fe) impact speed on wear of X38CrMoV5-1 steel in high pressure die casting conditions. *Wear* 424–425, 15–22. https://doi.org/10.1016/j.wear.2019.02.008.

Decker, R.F., Berman, T.D., Miller, V.M., Jones, J.W., Pollock, T.M., LeBeau, S.E. (2019). Alloy Design and Processing Design of Magnesium Alloys Using 2nd Phases. *JOM* 71, 2219–2226. https://doi.org/10.1007/s11837-019-03482-z.

Dobrzański, L.A., Król, M., Tański, T., Maniara, R. (2009). Effect of cooling rate on the solidification behavior of magnesium alloys. *ACMSSE* 1 (1), 21-24.

Dobrzański, L.A., Król, M., Tański, T. (2011). *Effect of cooling rate and aluminum contents on the MgAl-Zn alloys' structure and mechanical properties*. In *Effect of casting, plastic forming or surface technologies on the structure and properties of the selected engineering materials*. Volume 1, Open Access Library, pp. 9-54.

El Mahallawy, N., Ahmed Diaa, A., Akdesir, M., Palkowski, H. (2017). Effect of Zn addition on the microstructure and mechanical properties of cast, rolled and extruded Mg-6Sn-xZn alloys. *Mater. Sci. Eng. A* 680, 47–53. https://doi.org/10.1016/j.msea.2016.10.075

Godzierz, M., Olszówka-Myalska, A., Września, P. (2019). Wear resistance of composites with Mg-Zn-RE-Zr alloy matrix and open-celled carbon foam. *Mater. Eng.* 1, 16–22. https://doi.org/10.15199/28.2019.2.3.

He, M.L., Luo, T.J., Zhou, J.X., Yang, Y.S. (2018). Microstructure and mechanical properties of as-cast Mg-4Zn-0.5Zr-0.2Cu-0.2Ce alloy. *Mater. Sci. Technol.* 34 (11), 1370–1378. https://doi.org/10.1080/02670836.2018.1457288.

Jamesh, M.I., Wu, G., Zhao, Y., McKenzie, D.R., Bilek, M.M.M., Chu, P.K. (2015). Electrochemical corrosion behavior of biodegradable Mg–Y–RE and Mg–Zn–Zr alloys in Ringer's solution and simulated body fluid. *Corros. Sci.* 91, 160–184. https://doi.org/10.1016/j.corsci.2014.11.015.

Kapinos, D., Augustyn, B., Szymanek, M. (2014). Methods of introducing alloying elements into liquid magnesium. *Metall. Foundry Eng.* 40 (3), 141-160. https://doi.org/10.7494/mafe.2014.40.3.141.

Karakulak, E. (2019). A review: Past, present and future of grain refining of magnesium castings. *J. Magnes. Alloy* 7 (3), 355–369. https://doi.org/10.1016/j.jma.2019.05.001.

Kurnaz, S.C., Sevik, H., Açıkgöz, S., Özel, A. (2011). Influence of titanium and chromium addition on the microstructure and mechanical properties of squeeze cast Mg–6Al alloy. *J. Alloys Compd.* 509 (6), 3190–3196. https://doi.org/10.1016/j.jallcom.2010.12.055.

Li, Q., Wang, Q., Wang, Y., Zeng, X., Ding, W. (2007). Effect of Nd and Y addition on microstructure and mechanical properties of as-cast Mg–Zn–Zr alloy. *J. Alloys Compd.* 427 (1-2), 115–123. https://doi.org/10.1016/j.jallcom.2006.02.054.

Li, J., Lu, Y., Zhang, H., Xin, L. (2015). Effect of grain size and hardness on fretting wear behavior of Inconel 600 alloys. *Tribol. Int.* 81, 215–222. https://doi.org/10.1016/j.triboint.2014.08.005.

Mandal, D., Murmu, L., Choudhary, C., Singh, G., Sahoo, K.L. (2019). Influence of alloying elements and grain refiner on microstructure, mechanical and wear properties of Mg-Al-Zn alloys. *Can. Metall. Q.* 58 (2), 241–251. https://doi.org/10.1080/00084433.2018.1540087.

NovaCast (2020). Shell Mould Casting. Accessed 04.02.21. https://www.novacast.co.uk/services/casting/shell-mould-casting/.

Özarslan, S., Şevik, H., Sorar, İ. (2019). Microstructure, mechanical and corrosion properties of novel Mg-Sn-Ce alloys produced by high pressure die casting. *Mater. Sci. Eng. C* 105, 110064. https://doi.org/10.1016/j.msec.2019.110064.

Peterson Enterprises (2020). Graphite Mold Casting. Accessed 04.02.2021. http://www.petersonenterprises.com/processesproducts/casting/graphite-mold-casting.

Prabhu, D.B., Muthuraja, C., Nampoothiri, J., Gopalakrishnan, P., Ravi, K.R. (2018). Solidification Analysis of Mg–4Zn–xSr System to Study Phase Transformations in Mg-Rich Corner. *Trans. Indian Inst. Met.* 71, 2801–2806. https://doi.org/10.1007/s12666-018-1438-1.

Ren, Y.P, Guo, Y., Chen, D., Li, S., Pei, W.L., Qin, G.W. (2011). Isothermal section of Mg–Zn–Zr ternary system at 345 °C. *Calphad* 35 (3), 411–415. https://doi.org/10.1016/j.calphad.2011.05.009.

Shuai, C., Yang, Y., Wu, P., Lin, X., Liu, Y., Zhou, Y., Feng, P., Liu, X., Peng, S. (2017). Laser rapid solidification improves corrosion behavior of Mg-Zn-Zr alloy. *J. Alloys Compd.* 691, 961–969. https://doi.org/10.1016/j.jallcom.2016.09.019.

Snopiński, P., Król, M., Tański, T., Krupińska, B. (2018). Effect of cooling rate on microstructural development in alloy ALMG9. *J. Therm. Anal. Calorim.* 133, 379–390. https://doi.org/10.1007/s10973-018-7313-9.

Song, J., She, J., Chen, D., Pan, F. (2020). Latest research advances on magnesium and magnesium alloys worldwide. *J. Magnes. Alloys* 8 (1), 1–41. https://doi.org/10.1016/j.jma.2020.02.003.

Srinivasan, A., Huang, Y., Mendis, C.L., Blawert, C., Kainer, K.U., Hort, N. (2014). Investigations on microstructures, mechanical and corrosion properties of Mg–Gd–Zn alloys. *Mater. Sci. Eng.* A 595, 224–234. https://doi.org/10.1016/j.msea.2013.12.016.

Vinogradov, A., Orlov, D., Estrin, Y. (2012). Improvement of fatigue strength of a Mg–Zn–Zr alloy by integrated extrusion and equal-channel angular pressing. *Scripta Mater.* 67 (2) 209–212. https://doi.org/10.1016/j.scriptamat.2012.04.021.

Wang, C., Sun, M., Zheng, F., Peng, L., Ding, W. (2014). Improvement in grain refinement efficiency of Mg–Zr master alloy for magnesium alloy by friction stir processing. *J. Magnes. Alloys* 2 (3), 239–244. https://doi.org/10.1016/j.jma.2014.09.001.

Watarai, H. (2006). Trend of Research and Development for Magnesium Alloys. *Science and Technology Trends* 18, 84-97.

Wu, D., Chen, R.S., Tang, W.N., Han, E.H. (2012). Influence of texture and grain size on the room-temperature ductility and tensile behavior in a Mg–Gd–Zn alloy processed by rolling and forging. *Mater. Design* 41, 306–313. https://doi.org/10.1016/j.matdes.2012.04.033.

Yarkadaş, G., Kumruoğlu, L.C., Şevik, H. (2018). The effect of Cerium addition on microstructure and mechanical properties of high pressure die cast Mg-5Sn alloy. *Mater. Charact.* 136, 152–156. https://doi.org/10.1016/j.matchar.2017.11.057.

Yuan, Y., Huang, Y., Wei, Q. (2019). Effects of Zr Addition on Thermodynamic and Kinetic Properties of Liquid Mg-6Zn-xZr Alloys. *Metals* 9 (5), 607. https://doi.org/10.3390/met9050607.

Zhang, M., Chen, C., Liu, C., Wang, S. (2018). Study on Porous Mg-Zn-Zr ZK61 Alloys Produced by Laser Additive Manufacturing. *Metals* 8 (8), 635. https://doi.org/10.3390/met8080635.

Zhou, B., Liu, W., Wu, G., Zhang, L., Zhang, X., Ji, H., Ding, W. (2020). Microstructure and mechanical properties of sand-cast Mg-6Gd-3Y-0.5Zr alloy subject to thermal cycling treatment. *J. Mater. Sci. Technol.* 43, 208–219. https://doi.org/10.1016/j.jmst.2020.01.013.